Accounting for the Central Role of Interfacial Water in Protein-Ligand Binding Free Energy Calculations

Ido Y. Ben-Shalom[1], Zhixiong Lin[2], Brian K. Radak[2], Charles Lin[2], Woody Sherman[2], and Michael K. Gilson[1*]

[1]Skaggs School of Pharmacy and Pharmaceutical Sciences, University of California, San Diego, 92093 La Jolla, California, USA

[2]Silicon Therapeutics LLC, Boston, Massachusetts, 02110, USA

*To whom correspondence should be addressed, mgilson@health.ucsd.edu

1 ABSTRACT

Rigorous binding free energy methods in drug discovery are growing in popularity due to a combination of methodological advances, improvements in computer hardware, and workflow automation. These calculations typically use molecular dynamics (MD) to sample from the Boltzmann distribution of conformational states. However, when part or all the binding site is inaccessible to bulk solvent, the time needed for water molecules to equilibrate between bulk solvent and the binding site can be well beyond what is practical with standard MD. This sampling limitation is problematic in relative binding free energy calculations, which compute the reversible work of converting Ligand 1 to Ligand 2 within the binding site. Thus, if Ligand 1 is smaller and/or more polar than Ligand 2, the perturbation may allow additional water molecules to occupy a region of the binding site. However, this change in hydration may not be captured by standard MD simulations and may therefore lead to errors in the computed free energy. We recently developed a hybrid Monte Carlo/MD (MC/MD) method, which speeds the equilibration of water between bulk solvent and buried cavities, while sampling from the intended distribution of states. Here, we report on the use of this approach in the context of alchemical binding free energy calculations. We find that using MC/MD markedly improves the accuracy of the calculations and also reduces hysteresis between the forward and reverse perturbations, relative to matched calculations using only MD with or without the crystallographic water molecules. The present method is available for use in the AMBER simulation software.

2 INTRODUCTION

The identification of a small organic molecule that binds a targeted protein with high affinity is a key early challenge in many drug discovery projects. A range of computational methods to estimate the affinity of candidate drug molecules for proteins have been developed to assist at this stage.[1–3] In recent years, advancements in both computer hardware and software [4–10] have enabled increasing application of relatively detailed molecular simulations to this problem. In particular, building on fundamental work on both theory and methods,[11–18] it is now feasible to integrate rigorous free energy methods into the drug design process.[19–23]

Free energy methods require sampling the configurations of the aqueous protein-ligand complex from the Boltzmann distribution defined by a potential function, or force field.[24–26] These configurations are usually generated using molecular dynamics (MD) simulations,[27–30]

but Monte Carlo (MC) methods may also be employed.[31–33] Given a method that provides correct sampling of a molecular system at equilibrium, one may choose among several methods of computing the difference in the free energy between two states of the system. These methods include thermodynamic integration (TI),[34] free energy perturbation (FEP),[35] Bennett Acceptance Ratio,[36] which is closely related to FEP, and Multistate Bennett Acceptance Ratio (MBAR).[37] Perturbing all the way from the initial to the final state, although feasible in principle, usually leads to convergence problems, so it is common instead to compute the free energy difference by running equilibrium simulations at each of a series of small steps that interpolate between the initial and final states. Additional methods allow the calculation of free energy differences from nonequilibrium simulations, in which the progression from initial to final is forced to occur too fast for the simulations to generate equilibrium distributions.[38–42]

In the context of computer-aided drug design, free energy methods may be used to compute the standard free energy of binding [16] by interpolating between the bound and unbound states with steps along a physical pathway, in which the ligand is stepwise removed from the binding site,[14,43,44] or a non-physical, or alchemical, pathway, in which the ligand is artificially decoupled from the binding site and then recoupled with bulk solvent.[16,45,46] Such methods are often termed absolute binding free energy (ABFE) calculations to distinguish them from relative binding free energy (RBFE) calculations ,[11,21,22] which provide the difference in binding free energy of two chemically similar ligands by perturbing one into the other within the binding site and then in bulk solution, and then using thermodynamic closure to connect these differences with the difference between their binding free energies (Figure 1). Because converting one ligand to another is a non-physical process, RBFE calculations are also termed alchemical.

In some drug design projects, the crystal structure of the targeted binding pocket reveals a buried cavity that has no channel through which water can enter or exit. Thus, water in the pocket can exchange with bulk water only through conformational fluctuations that open the binding pocket. Such fluctuations are generally infrequent relative to the time scales accessible by current simulations. This situation poses a challenge for binding free energy calculations in which the hydration of the pocket should change on going from the initial to the final state. Thus, in alchemical ABFE calculations, decoupling of the ligand from the binding site leaves an empty binding pocket which usually should become hydrated. Similarly, when one uses alchemical RBFE methods to compare the binding free energy of two ligands of different size and/or polarity, the number of waters bound along with the ligand often ought to change. Commonly used MD simulations cannot replicate these changes in the hydration of buried

cavities, so the number of waters in the pocket remains constant, rather than adapting properly to changes in the ligand, and this structural error can lead to errors in computed free energies. In addition, if one runs the same perturbation in both directions — e.g., going from ligand 2 to ligand 1 instead of ligand 1 to ligand 2 — where the two starting states have different numbers of buried waters, the two free energies may be quite different. Such differences, termed hysteresis, are a sign of inadequate sampling in free energy calculations, as the free energy is a state function and the free energy change on going from state 1 to state 2 is the additive inversion of the free energy change on going from state 2 to state 1. Here the problem is inadequate sampling of water moves into and out of the binding site.

This problem can be addressed by including MC steps that can exchange water molecules into and out of the binding pocket without following a physically realizable path. When done with the correct Metropolis acceptance criterion,[47] the added MC steps should, like MD, sample from the desired thermodynamic distribution and thus rigorously yield the free energy. Early work along these lines mixed regular MD sampling with Grand Canonical (GC) MC steps, which add or remove water molecules to or from the system in a manner that preserves the thermodynamic distribution for the appropriate chemical potential of water.[48] The GC method has also been successfully applied to ligand binding free energies in the context of a purely MC algorithm,[49] and has been shown to reduce hysteresis when used to set up water occupancies along the perturbation steps of RBFE calculations.[50] A recent preprint also shows that a hybrid GC/MD approach yields less hysteresis and somewhat lower errors, relative to experiment, than pure MD, across a large number of test cases.[51]

We recently reported a combined MC/MD approach which equilibrates water between buried cavities and the bulk without requiring the Grand Canonical machinery and the resulting changes in particle number.[52] This method, which is available in the AMBER simulation package,[53] alternates blocks of standard MD steps with blocks of translational MC water move attempts executed within a rectangular region that overlaps with both the protein interior and the bulk solvent. The translational moves allow water molecules to exchange between bulk and buried cavities, while maintaining a Boltzmann distribution of states. In particular, water molecules can exit or enter the buried binding site as a ligand grows or contracts during the alchemical process of an RBFE calculation.

Here, we report the first application of the MC/MD method to the calculation of RBFEs for pairs of ligands that bind to buried protein cavities and that, when bound, are associated with different numbers of water molecules. We also compare this approach with other protocols

for handling binding site hydration, including methods based on standard MD simulations. The MC/MD approach yields notably lower hysteresis and better agreement with experiment.

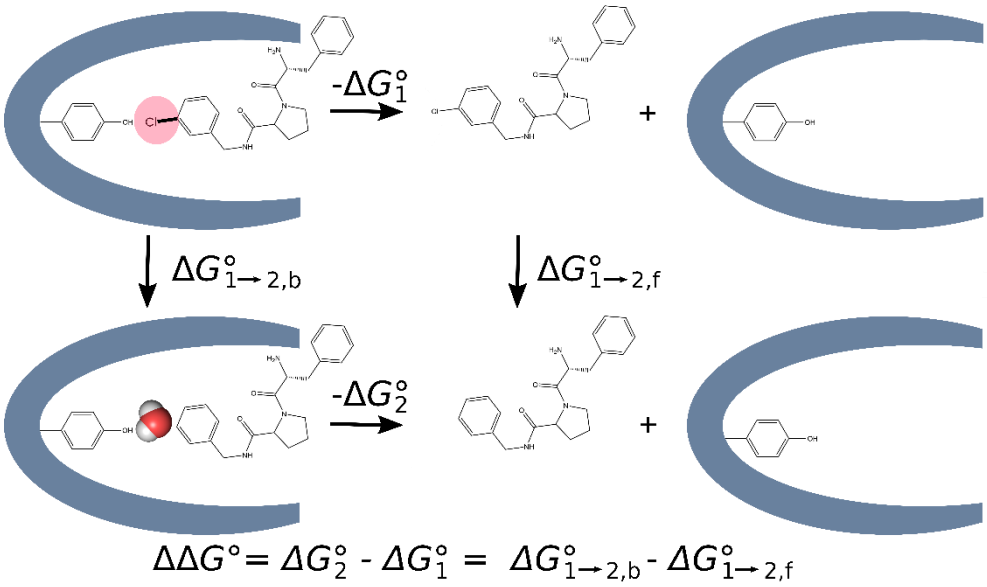

Figure 1: Diagram of the thermodynamic cycle used in relative binding free energy (RBFE=$\Delta\Delta G^{o}$) calculations where the hydration of the binding site differs between the two ligands. The RBFE is calculated as the difference between the free energies of converting Ligand 1 into Ligand 2 in the binding site versus in solution.

3 METHODS

3.1 OVERVIEW

We compared four methods of treating binding site hydration in calculations of RBFEs between paired ligands that occupy buried protein cavities. For each pair, one ligand is smaller than the other, and crystallographic data drawn from the Protein Data Bank (PDB)[54,55] indicates that the extra space associated with the smaller ligand is occupied by at least one additional buried water molecule (Section 3.2). Two of the methods (Methods 1 and 2) use our previously developed MC/MD code, which allows water molecules to equilibrate between bulk solvent and buried sites,[52] and two (Methods 3 and 4) use only standard MD. All four methods (Figure 2) follow the same overall protocol, starting from a crystal structure of the protein with one of the two ligands. They all carry out an initial water placement by the usual method of superimposing a pre-equilibrated box of water on the protein-ligand system and discarding waters that clash with the solutes. This hydrated system is then replicated to generate a separate simulation for each of a series of windows along the alchemical change of the initial ligand to

the final ligand, and the water structure in each of these simulations is allowed to relax with an equilibration simulation in which all non-hydrogen protein and ligand atoms are restrained to their initial coordinates. The progress from the initial to final window is scaled by the quantity λ, which goes from 0 to 1. Finally, production simulations with all atoms mobile are done for each λ window to compute the free energy change upon converting the initial ligand to the final ligand. Within this framework, the Methods are distinguished as follows.

Method 1 strips out the crystallographic waters before the initial hydration step and then uses MC/MD during both the equilibration step and the free energy production step. Thus, water occupancy is customized to each λ window during equilibration and can continue to vary within each window during production.

Method 2 is the same as Method 1, except that standard MD is used during the free energy production step. Thus, water occupancy is again customized to each λ window by the MC steps during equilibration, but it is fixed during production.

Method 3 also strips out the crystallographic waters before the initial hydration step but uses only standard MD during both the equilibration and production phases. Thus, water occupancy is determined by the initial hydration step and is the same for all λ windows, rather than being allowed to equilibrate between the binding cavity and the bulk as in Methods 1 and 2.

Method 4 is same as Method 3, except that crystallographic waters are retained.

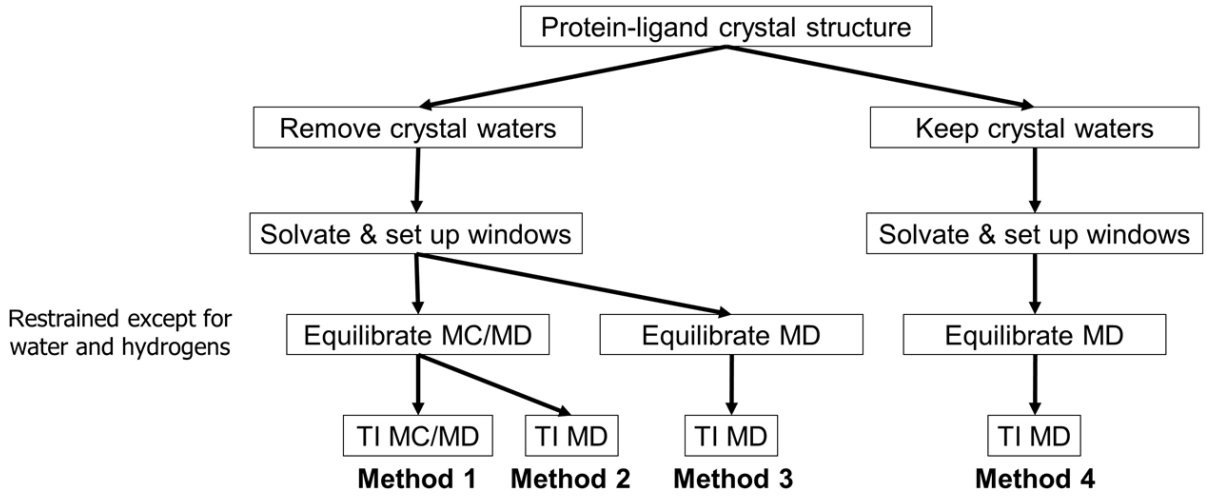

Figure 2: Diagram of the four methods of dealing with water molecules in the binding site. See text for details.

3.2 TEST SYSTEMS

Our test systems are pharmaceutically relevant protein-ligand systems that meet the following criteria: A) The binding pocket in crystal structures with bound ligand is a buried cavity; i.e., it has no channel to the bulk large enough to allow a water molecule to enter or exit. B) There are at least two inhibitors that share a chemical scaffold and differ from each other only by a small modification, and for which bound poses are available from crystal structures or could reasonably be constructed from existing co-crystal structures. C) Of these, we could find two ligands with different numbers of buried water molecules trapped between the ligand and protein. D) Experimentally measured binding free energies are available for both ligands. As detailed in Figure 3 and Table 1, the test systems are: Heat shock protein 90 (HSP90) with four ligands in two perturbations; Scytalone dehydratase and Bruton's tyrosine kinase (BTK), each with two ligands in one perturbation; Thrombin with four ligands in three perturbations; and OppA with four peptides in two perturbations. Here, we created ligand IDs comprising the first letter of the first author's surname followed by the identifier used for the molecule in the publication. The peptides are named according to the one letter code of the amino acids (Figure 3; Table 1). Co-crystal structures are not available for inhibitors D13b and C3d, but co-crystal structures are available for the other compounds in their perturbations (D15b in 4FCP and C5d in 5STD respectively). We constructed the required poses by docking D13b and C3d with the atoms they have in common with D15b and C5d, respectively, restrained to the available crystallographic coordinates.[56]

	Ligand 1		Ligand 2		
Protein	**Name**	**PDB ID**	**Name**	**PDB ID**	**N_{disp}; Figure 3 panel**
HSP90	D13b	4FCP[57*]	D15b	4FCQ[57]	1; A
	W1	2XAB[58]	W2	2XJG[58]	2; B
Scytalone dehydratase	C3d	5STD[59*]	C5d	3STD[59]	1; C
BTK	S8	4ZLZ[60]	S11	4Z3V[60]	1; D
Thrombin	B1b	2ZC9[61]	B5	2ZFF[61]	1; E
	B3a	2ZF0[61]			1; E
	B1a	2ZDV[61]			1; E
OppA	KKK	2OLB[62]	KWK	1JEV[63]	2; F
	KEK	1JEU[63]			4; F

Table 1: Ligands and proteins used to construct the present dataset. N_{disp}: the number of buried waters displaced in each perturbation, based on the crystal structures. Fig3 panel: panel in Figure 3 showing each perturbation. * indicates structures built from closely related ligands co-crystallized with the same protein.

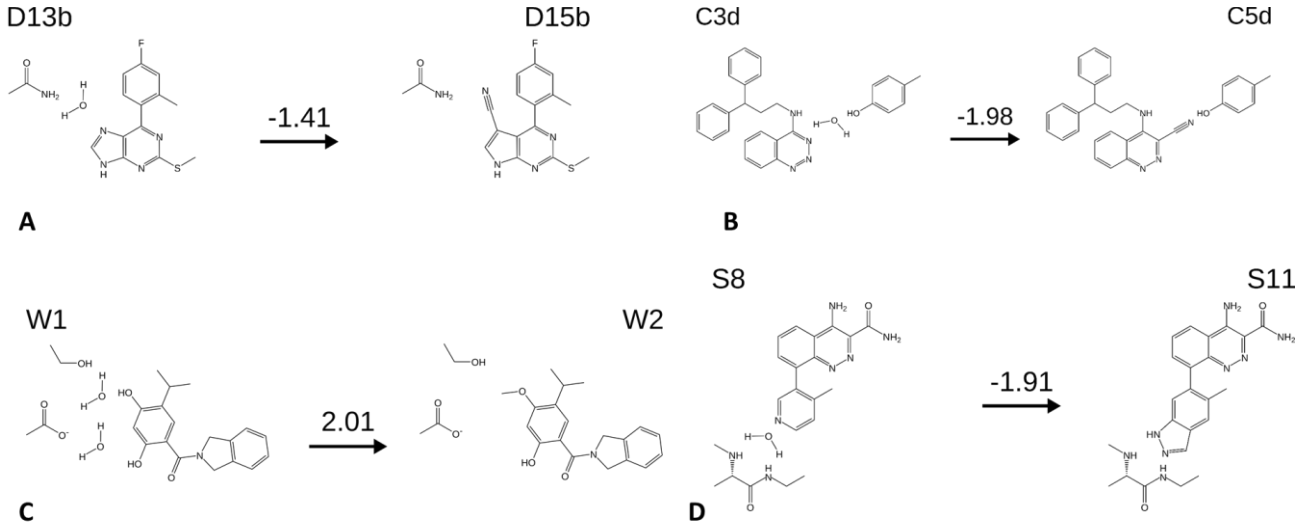

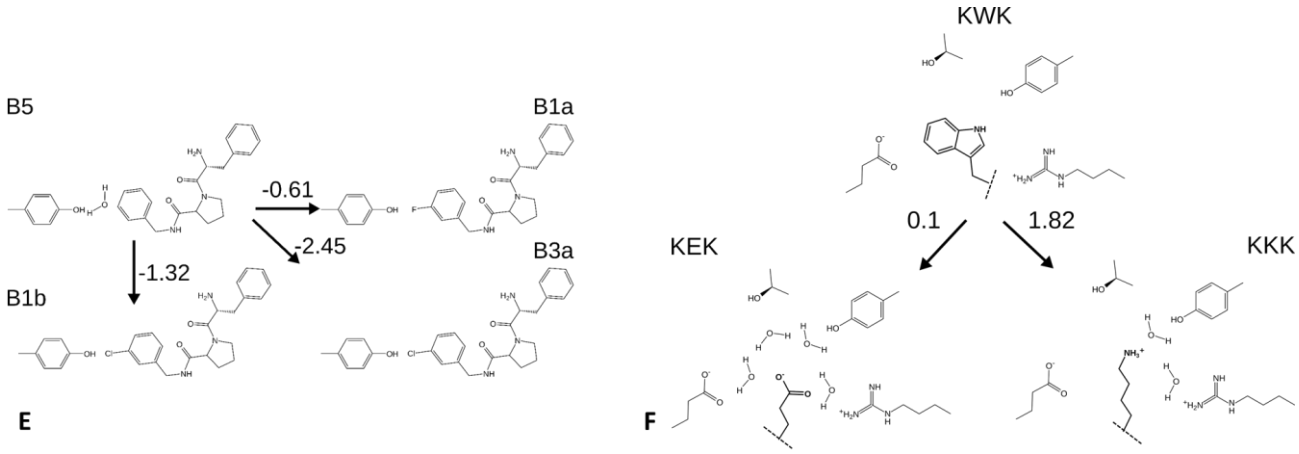

Figure 3: Perturbations considered in this study, with schematic representations of water displacements and selected neighboring side-chains. Numbers above arrows are the experimental free energy changes (kcal mol^{-1}). A, B) ligands D13b and D15b and W1 and W2, all HSP90 inhibitors. C) C3d and C5d, Scytalone dehydratase inhibitors. D) S8 and S11, BTK inhibitors. E) B1a, B1b, B3a, and B5, Thrombin inhibitors. F) peptides KEK, KKK, KWK, OppA inhibitors. Dashed lines indicate linkage to the rest of the peptide, which is not changed in these perturbations. Structures are shown with the charge states used in the simulations.

3.3 SIMULATIONS AND FREE ENERGY CALCULATIONS

All systems were constructed using the TIP3P water model[64], the ff14SB[65,66] force field for the protein, and GAFF2[67] for the ligands. Ligands and protein-ligand complexes were solvated in rectangular boxes using tleap, with initial buffer sizes of 12 and 8 Å, respectively. The net charge of each system was neutralized by addition of K+ or Cl- ions as appropriate. The simulations were performed on graphics processor units (GPUs) with AMBER18's GPU-accelerated PMEMD simulation code.[5,6,68,69] During equilibration, Cartesian restraints to the starting structure were applied to all ligand and protein heavy atoms, with a force constant of 5 kcal mol^{-1} Å^{-2}. After a brief minimization (50 steps of steepest descent plus 450 steps of conjugate gradient), the system was sequentially heated at a fixed volume with linear ramps joining the temperatures 5, 100, 200, and 298.15 K, at 20 ps per ramp, with each ramp followed by an additional 20 ps with pressure coupling. The resulting setups then were converted to alchemical topologies by mapping the initial ligand's atoms to the atoms of a new ligand, with a maximum common substructure algorithm as implemented in RDKit.[70] At this stage, the hydrogen masses were also increased to a target mass of 3.024 amu by repartitioning mass from the nearest bound heavy atom.[71,72] The heating steps were then repeated at each alchemical coupling value (λ window), and water structure was then equilibrated as described in Section 3.3. Restraints were then removed, and the production simulations were executed.

All simulations used a Langevin integrator with a 2 fs timestep for heating and equilibration and 4 fs for production, and a friction coefficient of 2 ps^{-1}. Heating steps were run in NVT, while equilibration and production steps were run in NPT with pressure regulated at 1 atm with a Monte Carlo barostat.[73] The SHAKE algorithm[74,75] was used to constrain hydrogen bond lengths, except when the bond involves a softcore atom; i.e., one that changes between the two end states.[76] The standard AMBER protocol for non-bonded interactions was followed. Thus, the particle mesh Ewald (PME) method[77] was used for periodic boundary conditions with an 8 Å cutoff for the short-ranged PME contribution as well as LJ interactions. A long-range continuum correction was used for the dispersive term.[78]

The TI free energy calculations were done in 3 stages[79]: decharge, Lennard-Jones (LJ), and recharge. At the outset, a common set of atoms between the two ligands is established. The atoms in each ligand outside this set are then labeled as the two "softcore regions". In the decharge stage, charge interactions only are removed from the first softcore region at λ windows of 0.0, 0.25, 0.5, 0.75, and 1.0. All interactions with the other ligand are neglected. During the LJ phase the repulsive/dispersive interactions on the first softcore region are turned off while those of the second region are turned on. The bonded and charge interactions in the common set of atoms are also switched at this time using λ windows of 0.0, 0.0479, 0.1151, 0.2063, 0.3161, 0.4374, 0.5626, 0.6839, 0.7937, 0.8849, 0.9521, and 1.0. The recharge stage uses the same protocol as the decharge stage except in reverse and using the second ligand. Note that, although we used TI[34,80,81], other methods, such as MBAR[37], could also be used in this protocol.

The reported RBFEs are calculated by subtracting the free energy of alchemically mutating the free ligand from the free energy of alchemically mutating the bound ligand (Figure 1). These are compared to experimental values (3.2Section 3.2). Each ligand pair was run in both directions, i.e., with each ligand playing the role of the starting ligand and the final ligand, to enable evaluation of the hysteresis. In addition, each of these calculations was run five times with different random number seeds, to enable evaluation of the variance. The reported RBFEs (Table 2) are averages over all 10 runs both for the free and the bound states:

$$\Delta\Delta G = \frac{1}{10}\left(\sum_{i=1}^{5}\left(\Delta G_{1\to 2,b,i} - \Delta G_{1\to 2,f,i}\right) - \sum_{i=1}^{5}\left(\Delta G_{2\to 1,b,i} - \Delta G_{2\to 1,f,i}\right)\right)$$

where $\Delta G_{1\to 2,x,i}$ is computed in the i^{th} of the five forward perturbations for the bound and free state x = b and x = f respectively, and $\Delta G_{2\to 1,x,i}$ is the corresponding backward perturbations, computed in the i^{th} of the five. (Note that the two directions give free energy differences of

opposite sign.) The hystereses and variances for the perturbations of the ligands in solution were small (average of ~0.1 kcal mol^{-1}) relative to those of those of the bound ligands, so the hystereses and variances of the reported RBFEs trace almost entirely to the bound state calculations, and we focus on the hysteresis for the bound states:

$$\text{Hysteresis} = \frac{1}{5}\left(\sum_{i=1}^{5} \Delta G_{1\rightarrow 2,b,i} + \sum_{i=1}^{5} \Delta G_{2\rightarrow 1,b,i}\right)$$

The reported standard deviations are computed separately for each group of five replicates (forward and backward) of the bound protein-ligand complex.

3.4 EQUILIBRATING BURIED WATER MOLECULES

The equilibration of buried water molecules was performed using our previously described MC/MD method which is implemented in AMBER.[52] In this method, the simulation alternates blocks of N_{MC} translational water move attempts with blocks of N_{MD} standard molecular dynamics time steps. As previously described, the MC moves occur only within a rectangular region that overlaps with the buried binding pocket and extends into bulk solvent (Figure 4). Here, the dimensions of this region were defined with a shift parameter of 8 Å as diagrammed in the figure. This is a conservative approach, which allows MC moves to translate water molecules into or out of any cavity that may exist or form throughout the protein. If one wishes to focus on equilibration of water between bulk and only the binding site, then a smaller box could be used. The rectangular region is filled with a steric grid that prevents move attempts into locations that are obviously blocked by other atoms. In order to allow moves into the binding pockets, we excluded the ligand from the steric grid. The MC blocks were performed at the same temperature as the MD, and at constant volume.

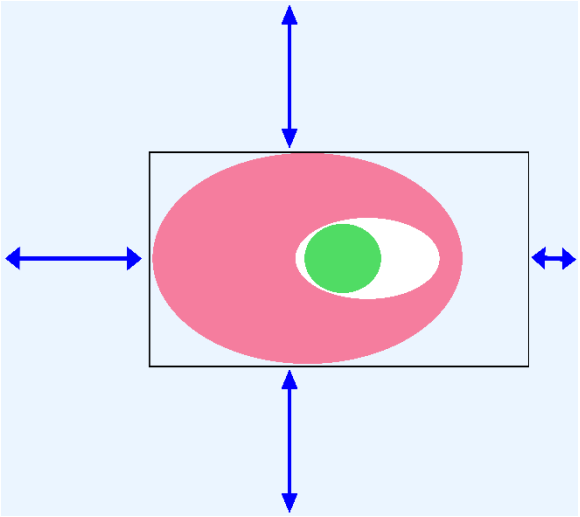

Figure 4: Schematic of the MC setup. Light blue: simulation box. Black rectangle: perimeter of the rectangular MC exchange region, with its steric grid. Pink and green are the protein and ligand respectively. The three longer arrows indicate the 8 Å shift of the grid from the edges of the simulation box. The short arrow on the right represents a smaller, 3 Å offset, which ensures that the box extends into bulk solvent and thus allows exchange between bulk and the interior of the protein.

Methods 1 and 2 (Section 3.1) used MC/MD during the equilibration stage. All heavy atoms of the protein and ligand were restrained, and alternating blocks of N_{MD} = 100 and $N_{MC} = 1\times10^5$ steps were carried out for a total of 25,000 MD time steps. Method 1 furthermore used MC/MD during the TI calculations, with N_{MD} = 1,000 and N_{MC} = 10,000. Methods 3 and 4 were the same except that no MC steps were carried out (N_{MC} = 0). Thus, Methods 2, 3, and 4 did not use MC/MD during the TI stage. This protocol was modified in two respects for the peptide ligands, because of the large size of these compounds and the greater magnitude of the perturbations. First, for only the equilibration step, we increased the total number of MD steps from 25,000 to 250,000, maintaining N_{MD} = 100, $N_{MC} = 1\times10^5$. Second, to speed water sampling in the region of interest, we excluded only the soft-core atoms from the steric grid, rather than the entire ligand as in the other perturbations. In this way, water moves into the binding pocket are attempted only at the specific site of the perturbation. Note, however, that the present protocol and grid specifications were not optimized for speed, and similar results may be obtainable with fewer MC steps. The compute time effectively required for an MC step here is about the same as that for an MD step.

4 RESULTS AND DISCUSSION

4.1 CALCULATION VERSUS EXPERIMENT

As indicated by the root-mean-square errors (RMSEs) in Table 1, Methods 1 and 2, which both use the MC/MD technology to equilibrate water occupancy in the binding sites, yield notably better agreement with experiment than do Methods 3 and 4, which do not allow waters to equilibrate between bulk and the binding sites. Note that the RMSE values exclude the results for KEK~KWK, for which all four methods yield errors of over 10 kcal mol^{-1}; this perturbation is examined separately in Section 4.3.3. As shown in the following subsection, the difference between Methods [1, 2] and Methods [3, 4] are large on the scale of the numerical uncertainties of the calculations. Thus, the present results support the utility of the MC/MD procedure as a tool to improve the accuracy of free energy calculations involving buried binding sites.

Interestingly, all of the benefit from using MC/MD is obtained by using it just for *initial* equilibration of water occupancy in each λ window (i.e. Method 2). That is, on-going equilibration of water occupancy in the course of the production calculations, as done in Method 1 but not Method 2, does not afford more accuracy, at least for the present cases. The two methods that use only MD, and thus that do not equilibrate water between the binding site and the bulk, give quite different results when crystallographic waters are kept in place (Method 4) versus when they are removed prior to initial solvation (Method 3). Indeed, these two methods yield free energies that differ by up to 18 kcal mol^{-1} (KWK~KKK, Table 2). Nonetheless, neither appears to be more significantly accurate than the other, based on their RMSE values of 4.1 and 3.6 kcal mol^{-1} (Table 2).

	Experiment	Method 1	Method 2	Method 3	Method 4
D13b~D15b	**1.41**	3.13	3.19	3.34	3.11
W1~W2	**2.01**	0.93	0.51	-4.64	2.80
C3d~C5d	**1.98**	3.24	2.59	3.69	1.32
S8~S11	**1.91**	3.35	3.99	4.92	-0.11
B1b~B5	**1.32**	1.99	1.82	1.86	1.29
B3a~B5	**2.45**	1.08	1.04	0.93	0.85
B1a~B5	**0.61**	0.99	0.86	0.65	2.95
KWK~KKK	**1.82**	0.12	0.49	10.22	-7.51
KEK~KWK	**0.10**	14.20	15.11	16.58	12.34
RMSE*		1.28	1.33	4.08	3.59

Table 2: Relative binding free energies (kcal mol^{-1}) of all perturbations considered here, and the root-mean-square error (RMSE) for each method, omitting the perturbation of KEK~KWK, as detailed in the main text.

4.2 NUMERICAL UNCERTAINTY AND HYSTERESIS

The mean standard deviations and hystereses of the free energy perturbations, computed as given in Section 3.3, are almost all smaller than the scale of the differences in accuracy between the methods which use MC/MD (Methods 1, 2) and those which use only MD (Methods 3, 4). Thus, the mean standard deviations are all in the range 0.84-0.94 kcal mol^{-1}, and the mean hystereses average 0.51-0.65 kcal mol^{-1}. (Note that KEK~KWK is again omitted from these statistics; see above.) The only exception is Method 4, whose mean hysteresis is larger, at 3.7 kcal mol^{-1}. It is not clear why retaining crystallographic waters, as done in Method 4, leads to greater hysteresis than omitting them and relying on the AMBER resolvation procedure (Method 3). These results support the significance of the observations in Section 4.1.

It is encouraging that most of the computed free energy differences are the same in both directions, as the free energy difference of a state change should be. However, it is worth emphasizing that low hysteresis does not imply good agreement with experiment. For example, the W1~W2 perturbation with Method 3 has zero hysteresis (Table 3) but deviates from the experimental value by 6.7 kcal mol^{-1} (Table 2).

	Method 1		**Method 2**		**Method 3**		**Method 4**	
	SD	Hyst	SD	Hyst	SD	Hyst	SD	Hyst
D13b~D15b	0.49	0.39	0.60	0.26	0.36	0.16	0.72	0.3
W1~W2	0.99	0.59	0.97	0.78	0.56	0.00	0.73	6.61
C3d~C5d	1.31	1.41	1.4	0.47	1.51	0.11	1.4	1.48
S8~S11	1.13	0.18	1.02	0.36	1.07	0.98	0.91	0.25
B1b~B5	0.45	0.41	0.38	0.08	0.46	0.05	0.41	1.91
B3a~B5	0.44	0.01	0.44	0.03	0.4	0.33	0.3	1.14
B1a~B5	0.32	0.5	0.32	0.49	0.3	0.19	0.29	1.12
KWK~KKK	1.58	1.91	1.57	1.41	1.43	2.05	1.16	14.37
KEK~KWK	1.51	0.45	1.79	0.93	1.42	0.74	1.65	6.22
Mean	**0.91**	**0.65**	**0.94**	**0.53**	**0.83**	**0.51**	**0.84**	**3.71**

Table 3: Standard deviations and hystereses (kcal mol^{-1}) associated with the relative binding free energy calculations considered here. See Section 3.3 for definitions. The KEK~KWK perturbations are omitted from the Means, as detailed in the main text.

4.3 CASE STUDIES

4.3.1 CHANGES IN WATER OCCUPANCY ALONG THE W1~W2 PERTURBATION

According to their respective co-crystal structures, going from ligand W1 (2XAB) to W2 (2XJG) is accompanied by displacement of two of three buried waters. We thus anticipated similar changes in the present perturbations. To check this, we examined the mean over the five replicates of the number of buried, ligand-associated waters in the last snapshot of the MC/MD equilibration phase for each λ window of this perturbation for the runs starting from W1 as well as those starting with W2. As seen in Figure 5 (left), which shows both Method 1 perturbations going from W1 on the left to W2 on the right, W1 does start with three water molecules, but the number fluctuates between about 1.5 and 3.0 in the early windows, falling to about 2.0 for most of the LJ windows, and then fluctuating between 1.5 and 2.0 as the charges become those of W2. The pattern is similar when water is allowed to equilibrate during the λ windows (Method 2), as shown in Figure 5 (right), which reports time-averaged water occupancy in each λ window. This similarity is consistent with the observation (Section 4.1) that Methods 1 and 2 give very similar free energies. The agreement between the water occupancy statistics between the two perturbation directions (red and blue in Figure 5) also helps explain the low hysteresis of these calculations.

We examined the electron density of the W2 co-crystal structure and confirmed the evidence for a single buried water associated with the ligand. Thus, the W2 simulations appear to overhydrate this structure. This could result from sampling issues, inaccuracies in the force field, and/or the fact that the crystallographic conditions (e.g., T = 100K) differ from those at which the binding affinities were measured and under which these simulations were, accordingly, carried out.

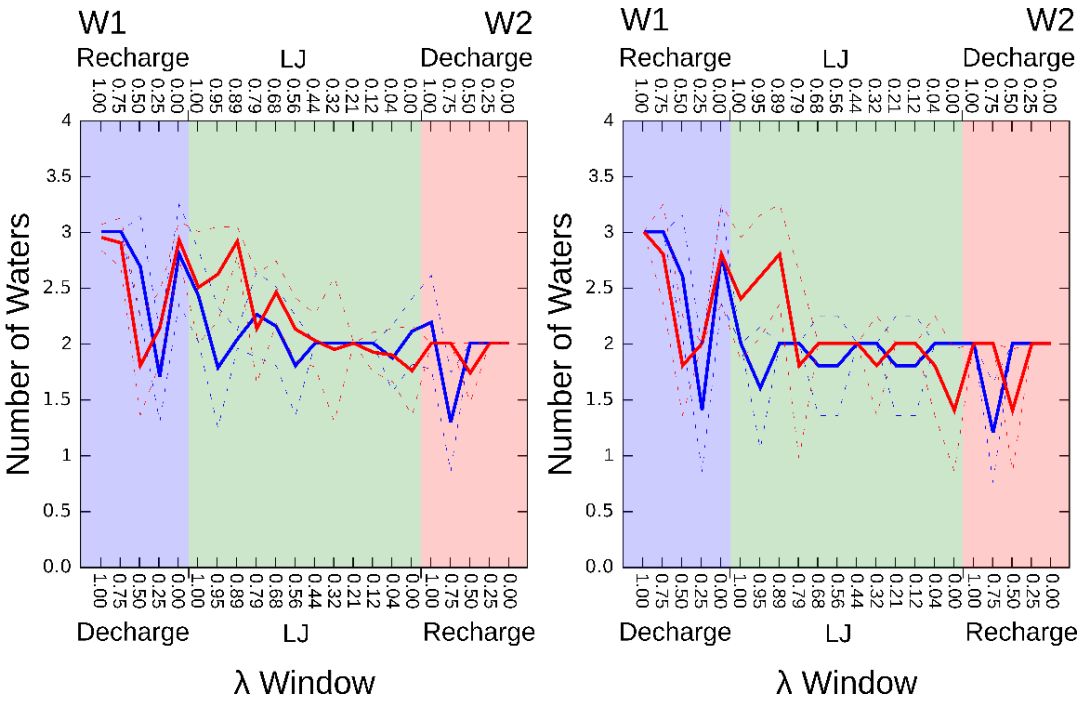

Figure 5: the number of buried water molecules in the perturbation of W1~W2 for each λ window, averaged over the 5 repetition of method 1. Right: the hydration state after the water equilibration step. Left: hydration state during the TI calculation. Blue is the perturbation W1→W2 with the λ windows labeled at the lower X-axis. Red is the reverse perturbation (W2→W1) with the λ windows in reverse order, labeled at the upper X-axis. Dashed lines show ranges defined by the standard deviations over the 5 repetitions.

4.3.2 WATER SITES IN HSP90

In contrast, the MC/MD calculations appeared to under-hydrate the structure of HSP90 with inhibitor D15b. Thus, the co-crystal structure (4FCQ[57]) has three buried water molecules, while the simulations placed only waters 1 and 2, as illustrated in Figure 6. In this case, however, examination of the electron density reveals that, although water sites 1 and 2 have distinct electron density, the electron density at water site 3 is less convincing, as shown in Figure 6. The electron density that was interpreted as a water appears to be continuous with the ligand density, rather than appearing as a discrete site. This might reflect partial occupancy by a different ligand, such as an impurity that may have been present in the mother liquor, or an

alternate conformation of either a ligand or protein component. In this case, then, the MC/MD calculation may offer a more realistic picture of hydration in the buried cavity.

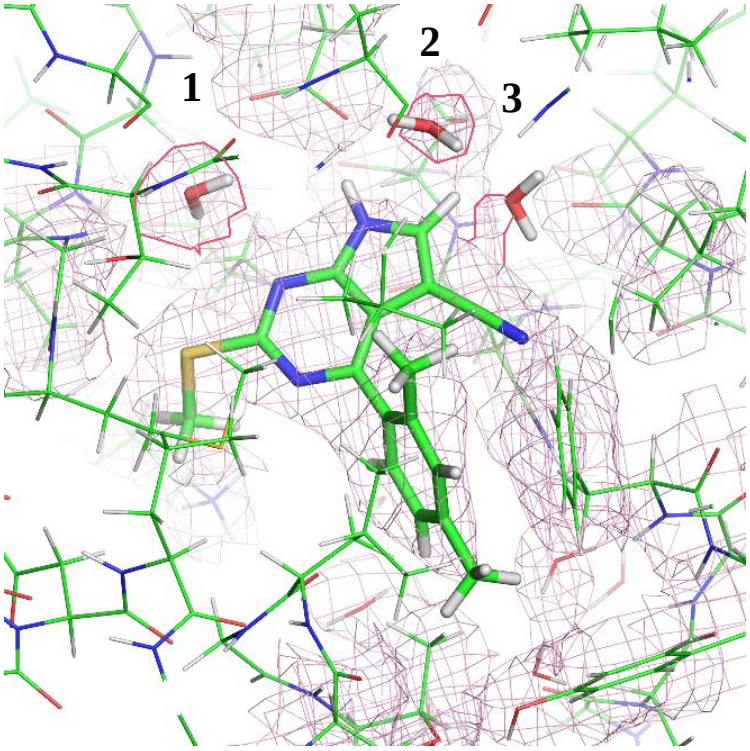

Figure 6: examining the electron density map of the 4FCQ reveals that the right most water molecule displays a strange shape (as if it is a part of the ligand), suggesting it to not be a water molecule.

4.3.3 THE KEK~KWK PERTURBATION

As noted in Section 4.1, the KEK~KWK perturbation is an extreme outlier, in the sense that none of the four methods tried here provides errors of less than 12 kcal mol^{-1}, relative to experiment. We therefore paid particular attention to how the MC/MD methods modeled the hydration. Going from KEK to KWK, the perturbation leads to displacement of four buried water molecules, according to the crystal structures (1JEU and 1JEV, respectively), and the electron density at the water sites appears to be well-resolved and distinct. We first examined the hydration states of the first decharge window ($\lambda = 0.0$) of KEK→KWK (Figure 7A) and the last recharge window ($\lambda = 1.0$) of KWK→KEK (Figure 7B). Both structures correspond to the fully present glutamic acid side chain and thus correspond to the co-crystal structure of KEK (1JEU).[63] As shown in the figure, the four crystallographic water sites are reasonably well replicated by the simulations, although one water molecule is notably displaced in B. The hydration states of the first decharge window of KWK→KEK (Figure 7C) and the last recharge window of KEK→KWK (Figure 7D), which both correspond to the fully present tryptophane

side chain, are compared with the co-crystal structure (1JEV, 2OLB) in panels C and D, respectively, of Figure 7. Here two out of three waters are properly placed.

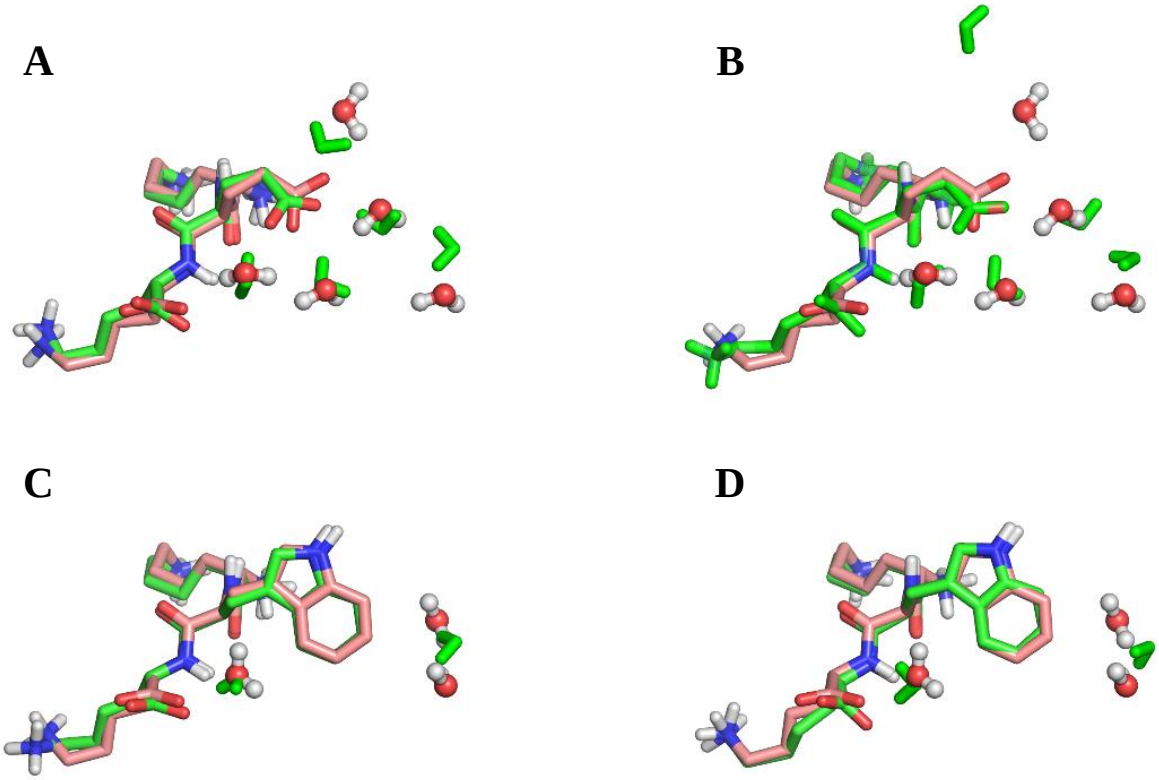

Figure 7: Crystal structures compared to the structures generated with MC/MD. For clarity, only the peptide KEK and the buried waters are shown. In A and B the crystal structure of the 1JEU is compared to A) the first window of the perturbation KEK→KWK (Decharge 0.0) and B) the last window of the perturbation KWK→KEK (Recharge 1.0). In C and D, the crystal structure of the 1JEV is compared to C) the first window of perturbation KWK→KEK (Decharge 0.0), and D) the last window of the perturbation KEK→KWK (Recharge 1.0).

Thus, although water placement by the MC/MD method does not agree perfectly with experiment, the deviations are on a similar scale to those of other perturbations for which the RBFE calculations were far more accurate. We therefore considered whether inadequate sampling might be to blame. However, extending the λ window production simulations ten-fold led to the same Method 1 result to within 0.1 kcal mol $^{-1}$. This does not rule out sampling as the problem, but it makes this less probable. We also compared the simulated conformational preferences of the peptide and protein with the conformations in the respective crystal structures and did not observe any notable rearrangements. It is also known that perturbations which, like this one, change the net charge of the system, can incur numerical errors on this basis, as previously discussed[82–86]. However, these technical issues are not expected to be large enough to account for the present error, and, indeed, the results for the other charge-changing

perturbation considered here, KWK~KKK, agree well with experiment when MC/MD is used (Table 2).

5 CONCLUSIONS

We find that allowing water molecules to equilibrate rapidly between bulk solvent and the protein interior, using the present hybrid MC/MD method, leads to more accurate RBFE calculations for ligands that occupy buried binding sites. For the systems studied here, the improvement, relative to pure MD, is ~2 kcal mol^{-1}, and the MC/MD results give accuracy to within ~1 kcal mol^{-1} of the experimental values, except for one case where all the methods fail. This method also improves the internal consistency of the calculations, in the sense that it reduces the hysteresis of free energies obtained from forward and reverse perturbations, which should give identical results. These improvements presumably derive from the ability of this method to allow the number of buried waters associated with the ligand to change in concert with the alchemical perturbation of the ligand. Examination of the numbers and positions of the simulated waters shows the anticipated changes, though the agreement between simulation and crystallographic water sites remains imperfect. This likely reflects some combination of issues with sampling, force field, and the fact that the simulated conditions (e.g., temperature) were chosen to model the conditions of the binding assays rather than of the crystallography experiments. Interestingly, the accuracy of the calculations run with pure MD was not affected by whether crystallographic waters were retained or deleted during setup of the simulations.

Although we focused on RBFE calculations, the present method is also expected to improve the accuracy of ABFE calculations involving ligands in buried binding sites, as recently highlighted.[87] In particular, double decoupling calculations [16] can leave the entire site empty without creating a channel to the bulk solvent. Allowing water to penetrate the site during the decoupling process may be essential to obtain accurate results. This is likely of less concern for ABFE calculations that follow physical pathways,[14,88] where forced removal of the ligand opens a channel to the bulk through which water can flow to reoccupy the site. However, there are cases where even these methods may benefit from the enhanced sampling of water, such as when a ligand is pulled from a deep, tunnel-like binding site that prevents water from back-filling until the ligand is entirely detached from the protein. Thus, there are a range of settings in which MC/MD and related methods should be of considerable value. The MC/MD implementation used here is available in current releases of the AMBER simulation package.

6 ACKNOWLEDGEMENTS

MKG acknowledges funding from National Institute of General Medical Sciences (GM061300 and GM100946). These findings are solely of the authors and do not necessarily represent the views of the NIH. MKG has an equity interest in and is a cofounder and scientific advisor of VeraChem LLC. ZL, BKR, CL and WS are employees of Silicon Therapeutics.

7 REFERENCES

(1) Yu, W.; MacKerell, A. D. Computer-Aided Drug Design Methods. In *Antibiotics*; Sass, P., Ed.; Methods in Molecular Biology; Springer New York: New York, NY, 2017; Vol. 1520, pp 85–106. https://doi.org/10.1007/978-1-4939-6634-9_5.

(2) Muegge, I.; Bergner, A.; Kriegl, J. M. Computer-Aided Drug Design at Boehringer Ingelheim. *J Comput Aided Mol Des* **2017**, *31* (3), 275–285. https://doi.org/10.1007/s10822-016-9975-3.

(3) Jain, A. Computer Aided Drug Design. *J. Phys.: Conf. Ser.* **2017**, *884*, 012072. https://doi.org/10.1088/1742-6596/884/1/012072.

(4) Susukita, R.; Ebisuzaki, T.; Elmegreen, B. G.; Furusawa, H.; Kato, K.; Kawai, A.; Kobayashi, Y.; Koishi, T.; McNiven, G. D.; Narumi, T.; Yasuoka, K. Hardware Accelerator for Molecular Dynamics: MDGRAPE-2. *Computer Physics Communications* **2003**, *155* (2), 115–131. https://doi.org/10.1016/S0010-4655(03)00349-7.

(5) Le Grand, S.; Götz, A. W.; Walker, R. C. SPFP: Speed without Compromise—A Mixed Precision Model for GPU Accelerated Molecular Dynamics Simulations. *Comput. Phys. Commun.* **2013**, *184* (2), 374–380. https://doi.org/10.1016/j.cpc.2012.09.022.

(6) Götz, A. W.; Williamson, M. J.; Xu, D.; Poole, D.; Le Grand, S.; Walker, R. C. Routine Microsecond Molecular Dynamics Simulations with AMBER on GPUs. 1. Generalized Born. *J. Chem. Theory Comput.* **2012**, *8* (5), 1542–1555. https://doi.org/10.1021/ct200909j.

(7) Eastman, P.; Friedrichs, M. S.; Chodera, J. D.; Radmer, R. J.; Bruns, C. M.; Ku, J. P.; Beauchamp, K. A.; Lane, T. J.; Wang, L.-P.; Shukla, D.; Tye, T.; Houston, M.; Stich, T.; Klein, C.; Shirts, M. R.; Pande, V. S. OpenMM 4: A Reusable, Extensible, Hardware Independent Library for High Performance Molecular Simulation. *J. Chem. Theory Comput.* **2013**, *9* (1), 461–469. https://doi.org/10.1021/ct300857j.

(8) Stone, J. E.; Hardy, D. J.; Ufimtsev, I. S.; Schulten, K. GPU-Accelerated Molecular Modeling Coming of Age. *Journal of Molecular Graphics and Modelling* **2010**, *29* (2), 116–125. https://doi.org/10.1016/j.jmgm.2010.06.010.

(9) Shaw, D. E.; Chao, J. C.; Eastwood, M. P.; Gagliardo, J.; Grossman, J. P.; Ho, C. R.; Ierardi, D. J.; Kolossváry, I.; Klepeis, J. L.; Layman, T.; McLeavey, C.; Deneroff, M. M.; Moraes, M. A.; Mueller, R.; Priest, E. C.; Shan, Y.; Spengler, J.; Theobald, M.; Towles, B.; Wang, S. C.; Dror, R. O.; Kuskin, J. S.; Larson, R. H.; Salmon, J. K.; Young, C.; Batson, B.; Bowers, K. J. Anton, a Special-Purpose Machine for Molecular Dynamics Simulation. In *Proceedings of the 34th annual international symposium on Computer architecture - ISCA '07*; ACM Press: San Diego, California, USA, 2007; p 1. https://doi.org/10.1145/1250662.1250664.

(10) Shaw, D. E.; Grossman, J. P.; Bank, J. A.; Batson, B.; Butts, J. A.; Chao, J. C.; Deneroff, M. M.; Dror, R. O.; Even, A.; Fenton, C. H.; Forte, A.; Gagliardo, J.; Gill, G.; Greskamp, B.; Ho, C. R.; Ierardi, D. J.; Iserovich, L.; Kuskin, J. S.; Larson, R. H.; Layman, T.; Lee, L.-S.; Lerer, A. K.; Li, C.; Killebrew, D.; Mackenzie, K. M.; Mok, S. Y.-H.; Moraes, M. A.; Mueller, R.; Nociolo, L. J.; Peticolas, J. L.; Quan, T.; Ramot, D.; Salmon, J. K.; Scarpazza, D. P.; Schafer, U. B.; Siddique, N.; Snyder, C. W.; Spengler, J.; Tang, P. T. P.; Theobald, M.; Toma, H.; Towles, B.; Vitale, B.; Wang, S. C.; Young, C. Anton 2: Raising the Bar for Performance and Programmability in a Special-Purpose Molecular Dynamics Supercomputer. In *SC14: International Conference for High Performance Computing, Networking, Storage and Analysis*; IEEE: New Orleans, LA, USA, 2014; pp 41–53. https://doi.org/10.1109/SC.2014.9.

(11) Tembre, B. L.; Mc Cammon, J. A. Ligand-Receptor Interactions. *Comput. Chem.* **1984**, *8* (4), 281–283. https://doi.org/10.1016/0097-8485(84)85020-2.

(12) Simonson, T.; Archontis, G.; Karplus, M. Free Energy Simulations Come of Age: Protein−Ligand Recognition. *Acc. Chem. Res.* **2002**, *35* (6), 430–437. https://doi.org/10.1021/ar010030m.
(13) Jorgensen, W. L.; Thomas, L. L. Perspective on Free-Energy Perturbation Calculations for Chemical Equilibria. *J. Chem. Theory Comput.* **2008**, *4* (6), 869–876. https://doi.org/10.1021/ct800011m.
(14) Woo, H.-J.; Roux, B. Calculation of Absolute Protein-Ligand Binding Free Energy from Computer Simulations. *Proceedings of the National Academy of Sciences* **2005**, *102* (19), 6825–6830. https://doi.org/10.1073/pnas.0409005102.
(15) Knight, J. L.; Brooks, C. L. λ-Dynamics Free Energy Simulation Methods. *J. Comput. Chem.* **2009**, *30* (11), 1692–1700. https://doi.org/10.1002/jcc.21295.
(16) Gilson, M. K.; Given, J. A.; Bush, B. L.; McCammon, J. A. The Statistical-Thermodynamic Basis for Computation of Binding Affinities: A Critical Review. *Biophys. J.* **1997**, *72* (3), 1047–1069. https://doi.org/10.1016/S0006-3495(97)78756-3.
(17) Kollman, Peter. Free Energy Calculations: Applications to Chemical and Biochemical Phenomena. *Chem. Rev.* **1993**, *93* (7), 2395–2417. https://doi.org/10.1021/cr00023a004.
(18) van Gunsteren, W. F.; Daura, X.; Mark, A. E. Computation of Free Energy. *Helvetica Chimica Acta* **2002**, *85* (10), 3113–3129. https://doi.org/10.1002/1522-2675(200210)85:10<3113::AID-HLCA3113>3.0.CO;2-0.
(19) Huggins, D. J.; Biggin, P. C.; Dämgen, M. A.; Essex, J. W.; Harris, S. A.; Henchman, R. H.; Khalid, S.; Kuzmanic, A.; Laughton, C. A.; Michel, J.; Mulholland, A. J.; Rosta, E.; Sansom, M. S. P.; van der Kamp, M. W. Biomolecular Simulations: From Dynamics and Mechanisms to Computational Assays of Biological Activity. *WIREs Comput Mol Sci* **2019**, *9* (3), e1393. https://doi.org/10.1002/wcms.1393.
(20) Bradshaw, R. T.; Dziedzic, J.; Skylaris, C.-K.; Essex, J. W. The Role of Electrostatics in Enzymes: Do Biomolecular Force Fields Reflect Protein Electric Fields? *J. Chem. Inf. Model.* **2020**, *60* (6), 3131–3144. https://doi.org/10.1021/acs.jcim.0c00217.
(21) Wang, L.; Wu, Y.; Deng, Y.; Kim, B.; Pierce, L.; Krilov, G.; Lupyan, D.; Robinson, S.; Dahlgren, M. K.; Greenwood, J.; Romero, D. L.; Masse, C.; Knight, J. L.; Steinbrecher, T.; Beuming, T.; Damm, W.; Harder, E.; Sherman, W.; Brewer, M.; Wester, R.; Murcko, M.; Frye, L.; Farid, R.; Lin, T.; Mobley, D. L.; Jorgensen, W. L.; Berne, B. J.; Friesner, R. A.; Abel, R. Accurate and Reliable Prediction of Relative Ligand Binding Potency in Prospective Drug Discovery by Way of a Modern Free-Energy Calculation Protocol and Force Field. *J. Am. Chem. Soc.* **2015**, *137* (7), 2695–2703. https://doi.org/10.1021/ja512751q.
(22) Cournia, Z.; Allen, B.; Sherman, W. Relative Binding Free Energy Calculations in Drug Discovery: Recent Advances and Practical Considerations. *J. Chem. Inf. Model.* **2017**, *57* (12), 2911–2937. https://doi.org/10.1021/acs.jcim.7b00564.
(23) Schindler, C.; Baumann, H.; Blum, A.; Böse, D.; Buchstaller, H.-P.; Burgdorf, L.; Cappel, D.; Chekler, E.; Czodrowski, P.; Dorsch, D.; Eguida, M.; Follows, B.; Fuchß, T.; Grädler, U.; Gunera, J.; Johnson, T.; Jorand Lebrun, C.; Karra, S.; Klein, M.; Kötzner, L.; Knehans, T.; Krier, M.; Leiendecker, M.; Leuthner, B.; Li, L.; Mochalkin, I.; Musil, D.; Neagu, C.; Rippmann, F.; Schiemann, K.; Schulz, R.; Steinbrecher, T.; Tanzer, E.-M.; Unzue Lopez, A.; Viacava Follis, A.; Wegener, A.; Kuhn, D. *Large-Scale Assessment of Binding Free Energy Calculations in Active Drug Discovery Projects*; preprint; 2020. https://doi.org/10.26434/chemrxiv.11364884.v2.
(24) Michel, J.; Essex, J. W. Prediction of Protein–Ligand Binding Affinity by Free Energy Simulations: Assumptions, Pitfalls and Expectations. *J Comput Aided Mol Des* **2010**, *24* (8), 639–658. https://doi.org/10.1007/s10822-010-9363-3.

(25) Christ, C. D.; Mark, A. E.; van Gunsteren, W. F. Basic Ingredients of Free Energy Calculations: A Review. *J. Comput. Chem.* **2009**, NA-NA. https://doi.org/10.1002/jcc.21450.
(26) Shirts, M. R.; Mobley, D. L. An Introduction to Best Practices in Free Energy Calculations. In *Biomolecular Simulations*; Monticelli, L., Salonen, E., Eds.; Humana Press: Totowa, NJ, 2013; Vol. 924, pp 271–311. https://doi.org/10.1007/978-1-62703-017-5_11.
(27) Mobley, D. L.; Gilson, M. K. Predicting Binding Free Energies: Frontiers and Benchmarks. *Annu. Rev. Biophys.* **2017**, *46*, 531–558. https://doi.org/10.1146/annurev-biophys-070816-033654.
(28) Karplus, M.; McCammon, J. A. Molecular Dynamics Simulations of Biomolecules. *Nat. Struct Biol.* **2002**, *9* (9), 646–652. https://doi.org/10.1038/nsb0902-646.
(29) Cole, D. J.; Tirado-Rives, J.; Jorgensen, W. L. Molecular Dynamics and Monte Carlo Simulations for Protein–Ligand Binding and Inhibitor Design. *Biochimica et Biophysica Acta (BBA) - General Subjects* **2015**, *1850* (5), 966–971. https://doi.org/10.1016/j.bbagen.2014.08.018.
(30) Michel, J.; Essex, J. W. Hit Identification and Binding Mode Predictions by Rigorous Free Energy Simulations. *J. Med. Chem.* **2008**, *51* (21), 6654–6664. https://doi.org/10.1021/jm800524s.
(31) Essex, J. W.; Severance, D. L.; Tirado-Rives, J.; Jorgensen, W. L. Monte Carlo Simulations for Proteins: Binding Affinities for Trypsin−Benzamidine Complexes via Free-Energy Perturbations. *J. Phys. Chem. B* **1997**, *101* (46), 9663–9669. https://doi.org/10.1021/jp971990m.
(32) Michel, J.; Verdonk, M. L.; Essex, J. W. Protein−Ligand Complexes: Computation of the Relative Free Energy of Different Scaffolds and Binding Modes. *J. Chem. Theory Comput.* **2007**, *3* (5), 1645–1655. https://doi.org/10.1021/ct700081t.
(33) Jorgensen, W. L.; Tirado-Rives, J. Molecular Modeling of Organic and Biomolecular Systems UsingBOSS AndMCPRO. *J. Comput. Chem.* **2005**, *26* (16), 1689–1700. https://doi.org/10.1002/jcc.20297.
(34) Kirkwood, J. G. *Theory of Liquids*; Gordon and Breach, 1968; Vol. Vol. 2.
(35) Zwanzig, R. W. High-Temperature Equation of State by a Perturbation Method. I. Nonpolar Gases. *The Journal of Chemical Physics* **1954**, *22* (8), 1420–1426. https://doi.org/10.1063/1.1740409.
(36) Bennett, C. H. Efficient Estimation of Free Energy Differences from Monte Carlo Data. *Journal of Computational Physics* **1976**, *22* (2), 245–268. https://doi.org/10.1016/0021-9991(76)90078-4.
(37) Shirts, M. R.; Chodera, J. D. Statistically Optimal Analysis of Samples from Multiple Equilibrium States. *The Journal of Chemical Physics* **2008**, *129* (12), 124105. https://doi.org/10.1063/1.2978177.
(38) Jarzynski, C. Equilibrium Free-Energy Differences from Nonequilibrium Measurements: A Master-Equation Approach. *Phys. Rev. E* **1997**, *56* (5), 5018–5035. https://doi.org/10.1103/PhysRevE.56.5018.
(39) Cossins, B. P.; Foucher, S.; Edge, C. M.; Essex, J. W. Protein−Ligand Binding Affinity by Nonequilibrium Free Energy Methods. *J. Phys. Chem. B* **2008**, *112* (47), 14985–14992. https://doi.org/10.1021/jp803533w.
(40) Sandberg, R. B.; Banchelli, M.; Guardiani, C.; Menichetti, S.; Caminati, G.; Procacci, P. Efficient Nonequilibrium Method for Binding Free Energy Calculations in Molecular Dynamics Simulations. *J. Chem. Theory Comput.* **2015**, *11* (2), 423–435. https://doi.org/10.1021/ct500964e.
(41) Gapsys, V.; Pérez-Benito, L.; Aldeghi, M.; Seeliger, D.; van Vlijmen, H.; Tresadern, G.; de Groot, B. L. Large Scale Relative Protein Ligand Binding Affinities Using Non-

Equilibrium Alchemy. *Chem. Sci.* **2020**, *11* (4), 1140–1152. https://doi.org/10.1039/C9SC03754C.
(42) Crooks, G. E. Nonequilibrium Measurements of Free Energy Differences for Microscopically Reversible Markovian Systems. 7.
(43) Velez-Vega, C.; Gilson, M. K. Overcoming Dissipation in the Calculation of Standard Binding Free Energies by Ligand Extraction. *J. Comput. Chem.* **2013**, n/a-n/a. https://doi.org/10.1002/jcc.23398.
(44) Gumbart, J. C.; Roux, B.; Chipot, C. Standard Binding Free Energies from Computer Simulations: What Is the Best Strategy? *J. Chem. Theory Comput.* **2013**, *9* (1), 794–802. https://doi.org/10.1021/ct3008099.
(45) Jorgensen, W. L.; Buckner, J. K.; Boudon, S.; Tirado-Rives, J. Efficient Computation of Absolute Free Energies of Binding by Computer Simulations. Application to the Methane Dimer in Water. *The Journal of Chemical Physics* **1988**, *89* (6), 3742–3746. https://doi.org/10.1063/1.454895.
(46) Boresch, S.; Karplus, M. The Jacobian Factor in Free Energy Simulations. *The Journal of Chemical Physics* **1996**, *105* (12), 5145–5154. https://doi.org/10.1063/1.472358.
(47) Metropolis, N.; Rosenbluth, A. W.; Rosenbluth, M. N.; Teller, A. H.; Teller, E. Equation of State Calculations by Fast Computing Machines. *J. Chem. Phys.* **1953**, *21* (6), 1087–1092. https://doi.org/10.1063/1.1699114.
(48) Woo, H.-J.; Dinner, A. R.; Roux, B. Grand Canonical Monte Carlo Simulations of Water in Protein Environments. *J. Chem. Phys.* **2004**, *121* (13), 6392–6400. https://doi.org/10.1063/1.1784436.
(49) Bruce Macdonald, H. E.; Cave-Ayland, C.; Ross, G. A.; Essex, J. W. Ligand Binding Free Energies with Adaptive Water Networks: Two-Dimensional Grand Canonical Alchemical Perturbations. *J. Chem. Theory Comput.* **2018**, *14* (12), 6586–6597. https://doi.org/10.1021/acs.jctc.8b00614.
(50) Wahl, J.; Smieško, M. Assessing the Predictive Power of Relative Binding Free Energy Calculations for Test Cases Involving Displacement of Binding Site Water Molecules. *J. Chem. Inf. Model.* **2019**, *59* (2), 754–765. https://doi.org/10.1021/acs.jcim.8b00826.
(51) Ross, G.; Russell, E.; Deng, Y.; Lu, C.; Harder, E.; Abel, R.; Wang, L. *Enhancing Water Sampling in Free Energy Calculations with Grand Canonical Monte Carlo*; preprint; 2020. https://doi.org/10.26434/chemrxiv.12595073.v1.
(52) Ben-Shalom, I. Y.; Lin, C.; Kurtzman, T.; Walker, R. C.; Gilson, M. K. Simulating Water Exchange to Buried Binding Sites. *J. Chem. Theory Comput.* **2019**, *15* (4), 2684–2691. https://doi.org/10.1021/acs.jctc.8b01284.
(53) D.A. Case, I.Y. Ben-Shalom, S.R. Brozell, D.S. Cerutti, T.E. Cheatham, III, V.W.D. Cruzeiro, T.A. Darden, R.E. Duke, D. Ghoreishi, M.K. Gilson, H. Gohlke, A.W. Goetz, D. Greene, R Harris, N. Homeyer, S. Izadi, A. Kovalenko, T. Kurtzman, T.S. Lee, S. LeGrand, P. Li, C. Lin, J. Liu, T. Luchko, R. Luo, D.J. Mermelstein, K.M. Merz, Y. Miao, G. Monard, C. Nguyen, H. Nguyen, I. Omelyan, A. Onufriev, F. Pan, R. Qi, D.R. Roe, A. Roitberg, C. Sagui, S. Schott-Verdugo, J. Shen, C.L. Simmerling, J. Smith, R. Salomon-Ferrer, J. Swails, R.C. Walker, J. Wang, H. Wei, R.M. Wolf, X. Wu, L. Xiao, D.M. York and P.A. Kollman. *Amber18*; University of California, San Francisco, 2018.
(54) Berman, H. M. The Protein Data Bank. *Nucleic Acids Research* **2000**, *28* (1), 235–242. https://doi.org/10.1093/nar/28.1.235.
(55) RCSB PDB www.rcsb.org.
(56) McGann, M. FRED and HYBRID Docking Performance on Standardized Datasets. *J Comput Aided Mol Des* **2012**, *26* (8), 897–906. https://doi.org/10.1007/s10822-012-9584-8.
(57) Davies, N. G. M.; Browne, H.; Davis, B.; Drysdale, M. J.; Foloppe, N.; Geoffrey, S.; Gibbons, B.; Hart, T.; Hubbard, R.; Jensen, M. R.; Mansell, H.; Massey, A.; Matassova,

N.; Moore, J. D.; Murray, J.; Pratt, R.; Ray, S.; Robertson, A.; Roughley, S. D.; Schoepfer, J.; Scriven, K.; Simmonite, H.; Stokes, S.; Surgenor, A.; Webb, P.; Wood, M.; Wright, L.; Brough, P. Targeting Conserved Water Molecules: Design of 4-Aryl-5-Cyanopyrrolo[2,3-d]Pyrimidine Hsp90 Inhibitors Using Fragment-Based Screening and Structure-Based Optimization. *Bioorganic & Medicinal Chemistry* **2012**, *20* (22), 6770–6789. https://doi.org/10.1016/j.bmc.2012.08.050.

(58) Woodhead, A. J.; Angove, H.; Carr, M. G.; Chessari, G.; Congreve, M.; Coyle, J. E.; Cosme, J.; Graham, B.; Day, P. J.; Downham, R.; Fazal, L.; Feltell, R.; Figueroa, E.; Frederickson, M.; Lewis, J.; McMenamin, R.; Murray, C. W.; O'Brien, M. A.; Parra, L.; Patel, S.; Phillips, T.; Rees, D. C.; Rich, S.; Smith, D.-M.; Trewartha, G.; Vinkovic, M.; Williams, B.; Woolford, A. J.-A. Discovery of (2,4-Dihydroxy-5-Isopropylphenyl)-[5-(4-Methylpiperazin-1-Ylmethyl)-1,3-Dihydroisoindol-2-Yl]Methanone (AT13387), a Novel Inhibitor of the Molecular Chaperone Hsp90 by Fragment Based Drug Design. *J. Med. Chem.* **2010**, *53* (16), 5956–5969. https://doi.org/10.1021/jm100060b.

(59) Chen, J. M.; Xu, S. L.; Wawrzak, Z.; Basarab, G. S.; Jordan, D. B. Structure-Based Design of Potent Inhibitors of Scytalone Dehydratase: Displacement of a Water Molecule from the Active Site ‡. *Biochemistry* **1998**, *37* (51), 17735–17744. https://doi.org/10.1021/bi981848r.

(60) Smith, C. R.; Dougan, D. R.; Komandla, M.; Kanouni, T.; Knight, B.; Lawson, J. D.; Sabat, M.; Taylor, E. R.; Vu, P.; Wyrick, C. Fragment-Based Discovery of a Small Molecule Inhibitor of Bruton's Tyrosine Kinase. *J. Med. Chem.* **2015**, *58* (14), 5437–5444. https://doi.org/10.1021/acs.jmedchem.5b00734.

(61) Baum, B.; Mohamed, M.; Zayed, M.; Gerlach, C.; Heine, A.; Hangauer, D.; Klebe, G. More than a Simple Lipophilic Contact: A Detailed Thermodynamic Analysis of Nonbasic Residues in the S1 Pocket of Thrombin. *Journal of Molecular Biology* **2009**, *390* (1), 56–69. https://doi.org/10.1016/j.jmb.2009.04.051.

(62) Tame, J. R.; Dodson, E. J.; Murshudov, G.; Higgins, C. F.; Wilkinson, A. J. The Crystal Structures of the Oligopeptide-Binding Protein OppA Complexed with Tripeptide and Tetrapeptide Ligands. *Structure* **1995**, *3* (12), 1395–1406. https://doi.org/10.1016/S0969-2126(01)00276-3.

(63) Tame, J. R. H.; Sleigh, S. H.; Wilkinson, A. J.; Ladbury, J. E. The Role of Water in Sequence-Independent Ligand Binding by an Oligopeptide Transporter Protein. *Nat Struct Mol Biol* **1996**, *3* (12), 998–1001. https://doi.org/10.1038/nsb1296-998.

(64) Jorgensen, W. L.; Chandrasekhar, J.; Madura, J. D.; Impey, R. W.; Klein, M. L. Comparison of Simple Potential Functions for Simulating Liquid Water. *J. Chem. Phys.* **1983**, *79* (2), 926–935. https://doi.org/10.1063/1.445869.

(65) Hornak, V.; Abel, R.; Okur, A.; Strockbine, B.; Roitberg, A.; Simmerling, C. Comparison of Multiple Amber Force Fields and Development of Improved Protein Backbone Parameters. *Proteins* **2006**, *65* (3), 712–725. https://doi.org/10.1002/prot.21123.

(66) Maier, J. A.; Martinez, C.; Kasavajhala, K.; Wickstrom, L.; Hauser, K. E.; Simmerling, C. Ff14SB: Improving the Accuracy of Protein Side Chain and Backbone Parameters from Ff99SB. *J. Chem. Theory Comput.* **2015**, *11* (8), 3696–3713. https://doi.org/10.1021/acs.jctc.5b00255.

(67) Wang, J.; Wolf, R. M.; Caldwell, J. W.; Kollman, P. A.; Case, D. A. Development and Testing of a General Amber Force Field. *J. Comput. Chem.* **2004**, *25* (9), 1157–1174. https://doi.org/10.1002/jcc.20035.

(68) Salomon-Ferrer, R.; Götz, A. W.; Poole, D.; Le Grand, S.; Walker, R. C. Routine Microsecond Molecular Dynamics Simulations with AMBER on GPUs. 2. Explicit Solvent Particle Mesh Ewald. *J. Chem. Theory Comput.* **2013**, *9* (9), 3878–3888. https://doi.org/10.1021/ct400314y.

(69) Mermelstein, D. J.; Lin, C.; Nelson, G.; Kretsch, R.; McCammon, J. A.; Walker, R. C. Fast and Flexible Gpu Accelerated Binding Free Energy Calculations within the Amber Molecular Dynamics Package. *J. Comput. Chem.* **2018**, *39* (19), 1354–1358. https://doi.org/10.1002/jcc.25187.
(70) Greg Landrum. *RDKit: Open-Source Cheminformatics*.
(71) Hopkins, C. W.; Le Grand, S.; Walker, R. C.; Roitberg, A. E. Long-Time-Step Molecular Dynamics through Hydrogen Mass Repartitioning. *J. Chem. Theory Comput.* **2015**, *11* (4), 1864–1874. https://doi.org/10.1021/ct5010406.
(72) Feenstra, K. A.; Hess, B.; Berendsen, H. J. C. Improving Efficiency of Large Time-Scale Molecular Dynamics Simulations of Hydrogen-Rich Systems. *Journal of Computational Chemistry* **1999**, *20* (8), 786–798. https://doi.org/10.1002/(SICI)1096-987X(199906)20:8<786::AID-JCC5>3.0.CO;2-B.
(73) Åqvist, J.; Wennerström, P.; Nervall, M.; Bjelic, S.; Brandsdal, B. O. Molecular Dynamics Simulations of Water and Biomolecules with a Monte Carlo Constant Pressure Algorithm. *Chemical Physics Letters* **2004**, *384* (4–6), 288–294. https://doi.org/10.1016/j.cplett.2003.12.039.
(74) Ryckaert, J.-P.; Ciccotti, G.; Berendsen, H. J. C. Numerical Integration of the Cartesian Equations of Motion of a System with Constraints: Molecular Dynamics of n-Alkanes. *J. Comput. Phys.* **1977**, *23* (3), 327–341. https://doi.org/10.1016/0021-9991(77)90098-5.
(75) Miyamoto, S.; Kollman, P. A. Settle: An Analytical Version of the SHAKE and RATTLE Algorithm for Rigid Water Models. *J. Comput. Chem.* **1992**, *13* (8), 952–962. https://doi.org/10.1002/jcc.540130805.
(76) Steinbrecher, T.; Mobley, D. L.; Case, D. A. Nonlinear Scaling Schemes for Lennard-Jones Interactions in Free Energy Calculations. *The Journal of Chemical Physics* **2007**, *127* (21), 214108. https://doi.org/10.1063/1.2799191.
(77) Darden, T.; York, D.; Pedersen, L. Particle Mesh Ewald: An N·log(N) Method for Ewald Sums in Large Systems. *J. Chem. Phys.* **1993**, *98* (12), 10089–10092. https://doi.org/10.1063/1.464397.
(78) Allen M. P. and Tildesley D. J. *Computer Simulation of Liquids*; Clarendon Press: Oxford, 1987.
(79) Song, L. F.; Lee, T.-S.; Zhu, C.; York, D. M.; Merz, K. M. Using AMBER18 for Relative Free Energy Calculations. *J. Chem. Inf. Model.* **2019**, *59* (7), 3128–3135. https://doi.org/10.1021/acs.jcim.9b00105.
(80) Lee, T.-S.; Cerutti, D. S.; Mermelstein, D.; Lin, C.; LeGrand, S.; Giese, T. J.; Roitberg, A.; Case, D. A.; Walker, R. C.; York, D. M. GPU-Accelerated Molecular Dynamics and Free Energy Methods in Amber18: Performance Enhancements and New Features. *J. Chem. Inf. Model.* **2018**, *58* (10), 2043–2050. https://doi.org/10.1021/acs.jcim.8b00462.
(81) Lee, T.-S.; Hu, Y.; Sherborne, B.; Guo, Z.; York, D. M. Toward Fast and Accurate Binding Affinity Prediction with PmemdGTI: An Efficient Implementation of GPU-Accelerated Thermodynamic Integration. *J. Chem. Theory Comput.* **2017**, *13* (7), 3077–3084. https://doi.org/10.1021/acs.jctc.7b00102.
(82) Rocklin, G. J.; Mobley, D. L.; Dill, K. A.; Hünenberger, P. H. Calculating the Binding Free Energies of Charged Species Based on Explicit-Solvent Simulations Employing Lattice-Sum Methods: An Accurate Correction Scheme for Electrostatic Finite-Size Effects. *The Journal of Chemical Physics* **2013**, *139* (18), 184103. https://doi.org/10.1063/1.4826261.
(83) Wallace, J. A.; Shen, J. K. Charge-Leveling and Proper Treatment of Long-Range Electrostatics in All-Atom Molecular Dynamics at Constant PH. *The Journal of Chemical Physics* **2012**, *137* (18), 184105. https://doi.org/10.1063/1.4766352.

(84) Lin, Y.-L.; Aleksandrov, A.; Simonson, T.; Roux, B. An Overview of Electrostatic Free Energy Computations for Solutions and Proteins. *J. Chem. Theory Comput.* **2014**, *10* (7), 2690–2709. https://doi.org/10.1021/ct500195p.
(85) Reif, M. M.; Oostenbrink, C. Net Charge Changes in the Calculation of Relative Ligand-Binding Free Energies via Classical Atomistic Molecular Dynamics Simulation. *J. Comput. Chem.* **2014**, *35* (3), 227–243. https://doi.org/10.1002/jcc.23490.
(86) Chen, W.; Deng, Y.; Russell, E.; Wu, Y.; Abel, R.; Wang, L. Accurate Calculation of Relative Binding Free Energies between Ligands with Different Net Charges. *J. Chem. Theory Comput.* **2018**, *14* (12), 6346–6358. https://doi.org/10.1021/acs.jctc.8b00825.
(87) Cournia, Z.; Allen, B. K.; Beuming, T.; Pearlman, D. A.; Radak, B. K.; Sherman, W. Rigorous Free Energy Simulations in Virtual Screening. *J. Chem. Inf. Model.* **2020**, acs.jcim.0c00116. https://doi.org/10.1021/acs.jcim.0c00116.
(88) Henriksen, N. M.; Fenley, A. T.; Gilson, M. K. Computational Calorimetry: High-Precision Calculation of Host–Guest Binding Thermodynamics. *J. Chem. Theory Comput.* **2015**, *11* (9), 4377–4394. https://doi.org/10.1021/acs.jctc.5b00405.

for Table of Contents use only

Accounting for the Central Role of Interfacial Water in Protein-Ligand Binding Free Energy Calculations

Ido Y. Ben-Shalom, Zhixiong Lin, Brian K. Radak, Charles Lin, Woody Sherman, and Michael K. Gilson